

# Aggregation and sticking probability of gold on tungsten trioxide films

L.J. LeGore<sup>a,\*</sup>, R.J. Lad<sup>a</sup>, J.F. Vetelino<sup>a</sup>, B.G. Frederick<sup>a</sup>, E.A. Kenik<sup>b</sup>

<sup>a</sup>Laboratory for Surface Science and Technology, University of Maine, Orono, ME 04469, USA

<sup>b</sup>Metals and Ceramics Division, Oak Ridge National Laboratory, Oak Ridge, TN 37831, USA

## Abstract

Both scanning electron microscopy (SEM) and transmission electron microscopy (TEM) images show that gold layers, 0.8–3.2 nm thick, deposited on WO<sub>3</sub> films aggregate into particles at temperatures above 400°C. The particles increase in size while the number density decreases over time. Particle size distributions indicate that the growth mechanism is coalescence due to island mobility rather than Ostwald ripening. Both SEM and X-ray photoemission spectroscopy (XPS) analysis indicate that the amount of gold deposited on the surface is approximately 50% of the value as determined by the quartz crystal monitor (QCM) during deposition. This difference is believed to be due to a low initial sticking probability of gold on the WO<sub>3</sub> surface during deposition. Finding means to create and stabilize metal particles of the optimum size remains a problem in the fields of catalysis and gas sensors. © 2001 Elsevier Science B.V. All rights reserved.

**Keywords:** Tungsten trioxide; Gold catalyst; Particle coalescence; Gas sensors

## 1. Introduction

Metals are frequently added to the surface of metal oxide sensing films in order to increase sensitivity and selectivity to the analyte gas [1,2]. In particular, gold has been added to WO<sub>3</sub> to improve the detection of hydrogen sulfide [3–6]. The amount of metal added is typically a few monolayers equivalent and exists on the surface as isolated particles or islands.

Several factors must be considered in the design of sensors with catalytic metal additives. First, the reactivity of small particles can depend upon particle size, and changes in particle size may lead to different product distributions or reaction rates [7]. The origin of particle size effects has been the subject of investigations in heterogeneous catalysis for more than three decades [7,8]. A more recent study by Goodman et al. has indicated that the important parameter may be the thickness of the metal layer [9]. In their study, gold clusters with a thickness of two atoms exhibited a band gap uncharacteristic of bulk metals and were shown to be particularly suited for catalyzing the oxidation of CO.

Second, the particle size may affect the sensing mechanism. Since the decomposition of hydrocarbons can lead to intermediate species which must diffuse from the metal cluster to the oxide surface, better transport between particles and the oxide is expected for smaller particles. The

larger surface area of large particles might be expected to accelerate the oxidation of a reducing gas but the products of the reaction would likely return to the atmosphere with little influence on the conductivity of the supporting oxide [10]. The processes which occur near the metal/oxide interface, such as spillover of dissociated adsorbed molecules from the metal to the oxide, are the ones likely to affect the oxide conductivity [4]. This dissociation and “spillover” can occur for both oxygen and reducing gas molecules [11]. If the metal/oxide interface is important, then it follows that this region should be maximized by decreasing the particle size and increasing their number density.

Third, metal adlayers often exhibit aggregation or coarsening, resulting in the mean particle size growing irreversibly with time, and a corresponding decrease in number density. This process is driven by an overall decrease in the surface free energy. The aggregation can occur by two different mechanisms [12]. In Ostwald ripening, particles exchange atoms by surface diffusion leading to the growth of particles larger than a critical radius at the expense of particles smaller than the critical radius. In coalescence, entire particles diffuse on the surface where they collide and coalesce into larger particles. While there is no existing data for gold on WO<sub>3</sub>, this coarsening process has been reported for a number of metal/substrate systems: Pd on WO<sub>3</sub> [13], Au on glass [14], TiO<sub>2</sub> [15],  $\alpha$ -C and SiO [16,17], Ga, Sn, and Ge on Si [18,19], and Ag on mica [20]. As may be expected, cluster mobility has been shown to be substrate dependent [17,21]. While the process is accelerated at

\* Corresponding author.

E-mail address: jay.legore@maine.edu (L.J. LeGore).

elevated temperatures, it has been observed at room temperature [22,23]. Since sensing films are operated at temperatures as high as 300°C or more, it is possible for the morphology of the metal particles to change with time, causing drift in gas sensitivity [24]. Extensive efforts in the field of catalysis have been expended in order to find ways to stabilize small metal particles. Recent work in surface science has focused upon stabilizing small particles at defects, such as steps, on single crystal surfaces [25,26]. Finding means to create and stabilize metal particles of the optimum size remains a problem.

Xu and Goodman have reported the possibility of significant error in estimated deposition rates as measured by quartz crystal monitor (QCM) due to the low initial sticking probability of copper on SiO<sub>2</sub> [27]. The initial sticking probability varied from 0.6 at 100 K to 0.1 above 400 K. A similar finding has been reported for Cu on SiO<sub>2</sub> and Cu on MgO at 300 K [28]. This behavior was considered anomalous because most metals with low vapor pressures adsorb on solid surfaces with unity sticking coefficient at 300 K.

These authors [28] proposed that the low sticking coefficient is due to the closed d-shell of the Cu and the closed-shell nature of the substrate. Similar low sticking coefficients on oxides were predicted for metals with similar chemical properties, such as Ag and Au.

For the work reported here, a number of experiments were performed in order to study the effect of time and temperature on the structure of surface gold on films of WO<sub>3</sub>. The morphology and crystal structure of the WO<sub>3</sub> films, grown on r-cut sapphire (Al<sub>2</sub>O<sub>3</sub> (1 0  $\bar{1}$  2)) substrates, is described elsewhere [29]. Scanning electron microscopy (SEM) and transmission electron microscopy (TEM) images were used to determine the size and number density of surface particles. Gold volume was also calculated from X-ray photoemission spectroscopy (XPS) peak area ratios.

The gold particles are found to increase in size while the number density decreases over time at temperatures above 400°C. Particle size distributions indicate that the growth mechanism is coalescence due to island mobility rather than Ostwald ripening. The amount of gold deposited on the surface, as determined by both SEM and XPS, is approximately 50% of the value as determined by the QCM during deposition. This difference is believed to be due to a low initial sticking probability of gold on the WO<sub>3</sub> surface during deposition.

## 2. Experimental

The WO<sub>3</sub> films were prepared by reactive RF magnetron sputtering using a deposition temperature of 200°C and an Ar/O<sub>2</sub> of 50/50 as described elsewhere [29]. Gold was added by dc magnetron sputtering, also at a deposition temperature of 200°C. The sample designation defined for each WO<sub>3</sub> thickness, gold thickness, and analysis method are shown in

Table 1  
Sample designation for gold aggregation study

Sample	WO <sub>3</sub> thickness (nm)	Gold thickness (nm)	Analysis
A	100	0.8	SEM
B	100	1.6	SEM
C	100	3.2	SEM
D	500	1.5	TEM
E	500	1.5	XPS

Table 1. The amount of gold was determined by the QCM with the assumption that the sticking coefficient was the same for impingement of gold on the QCM and on the WO<sub>3</sub> film.

The samples A, B, and C were heated in a tube furnace in air and SEM images of the surface of all of the films were taken after 3 h at 400°C, 16 h at 400°C, and 7 h at 600°C. These temperatures are higher than the typical operating temperature used for a WO<sub>3</sub> film sensing application [6,30] but were chosen to simulate accelerated aging. Sample D was heated in air for 1 h at 400°C and was examined with TEM after back thinning.

Sample E was examined using XPS at 20°C, and again after annealing for 20 h at 440°C and 3.5 h at 560°C, all under UHV conditions. The W 4f and Au 4f peaks were recorded at the beginning and the end of this annealing process.

## 3. Results and discussion

### 3.1. Surface aggregation

The effects of aggregation of gold on WO<sub>3</sub> films are illustrated by SEM images of sample C, taken after each of the three annealing periods, as shown in Fig. 1. The gold particles on the surface produce high contrast and can easily be seen as bright regions. These images clearly show that the gold particles increase in size and that the number density decreases with annealing.

These images and others were analyzed with Image SXM [31] a modification of NIH Image.<sup>1</sup> A macro which performed background subtraction and filtering was run for each image [32]. The macro also includes a threshold function which converts the gray scale image into a black and white binary file. An example of a processed image is shown in Fig. 2a, which can be compared to the unprocessed image in Fig. 1c. An outline of the particles generated from the black and white image was overlaid on the unprocessed image as shown in Fig. 2b. This illustrates the effectiveness of the software in identifying the particle boundaries. As can

<sup>1</sup> The public domain NIH Image program was developed at the US National Institutes of Health and is available on the Internet at <http://rsb.info.nih.gov/nih-image/>.

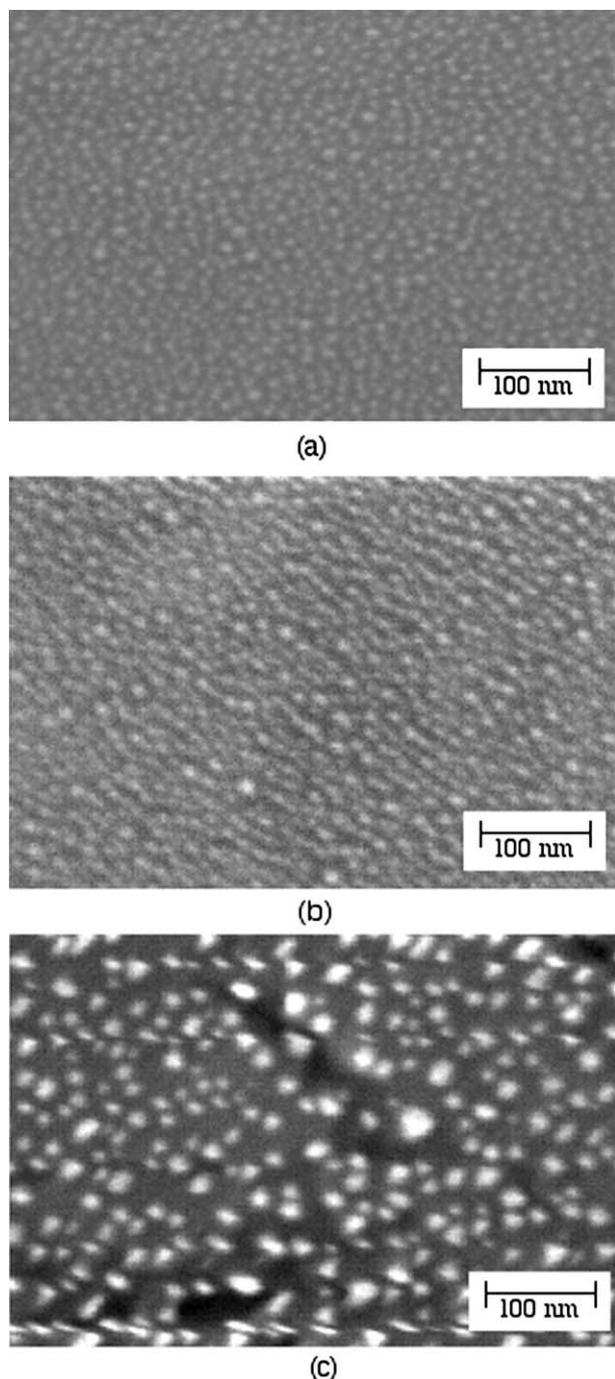


Fig. 1. SEM images of 3.2 nm surface gold on a  $\text{WO}_3$  film (a) after 3 h at  $400^\circ\text{C}$ ; (b) after an additional 13 h at  $400^\circ\text{C}$ ; (c) after an additional 7 h at  $600^\circ\text{C}$ .

be seen, some particles are connected in the processed image which are not connected in the unprocessed image. A minimum and maximum particle size (in pixels) was chosen from the unconnected particles. The software then counted the number of particles in this range and the area of each particle. This process was then repeated for the remaining particles larger than the previously chosen maximum (assumed to be connected particles). The average area of

the particles counted in the first pass was divided into the total area from the second pass. This number was used as the number of connected particles and was added to the number of unconnected particles to produce the total number of particles.

A TEM image of sample D is shown in Fig. 3. The small black regions, 3–15 nm in diameter, are attributed to gold particles. These features are not seen in TEM images of similar films with no surface gold. The particle sizes and number density were measured for a representative area of this image. The results of the above analysis are shown in Table 2, which gives an estimate of the changes in number density and particle size during the annealing process.

If the particles are assumed to be approximately hemispherical in shape and the area of each particle in the image is assumed to be the area of the hemisphere's base, then a volume for each particle can be calculated. The hemispherical assumption has been made in a scanning tunneling microscopy study of Pd cluster on  $\text{WO}_3$  [13]. Where the data is available, the average volume growth rate of the particles can be calculated. For sample C, the growth rate is  $7.8 \text{ nm}^3/\text{h}$  at  $400^\circ\text{C}$  and  $95 \text{ nm}^3/\text{h}$  at  $600^\circ\text{C}$ . Assuming an Arrhenius dependence, the activation energy can be estimated to be 0.6 eV from this data [19]. This value is within the range reported for Ga, Sn, and Ge on Si (0.3–1.0 eV) [18,19], Au on glass (0.5 eV) [14], and Ag on mica (0.5 eV) [20].

The two models for particle growth predict different particle size distributions. Size distributions can therefore be used as an aid in determining which mechanism is operable for a given metal/substrate system. Two distributions are predicted for Ostwald ripening based on whether the rate limiting step is either surface diffusion or transfer at the particle/substrate interface [33]. A single distribution with one fitting parameter, based on the functional dependence of the diffusion coefficient on the particle size, has been developed for coalescence. Both models assume the distribution is time invariant after the initial deposition and nucleation phase, i.e. the distribution is independent of temperature and time. The three model distribution functions along with the data are plotted in Fig. 4. The data point for each normalized radius is the mean of 10 measurements on five samples. The normalized radius is the particle radius divided by the average particle radius at a given time. As can be seen in this figure, the data is modeled best by coalescence.

### 3.2. Gold volume and initial sticking

The actual volume of gold was estimated using both SEM and XPS methods. By comparing the results with the volume measured by the QCM during deposition, an estimate of the initial sticking probability (sticking coefficient) for gold on  $\text{WO}_3$  can be made.

After the volume of each particle was calculated from an SEM image, the volumes were summed for the entire image and a volume of gold per unit area found. This can be

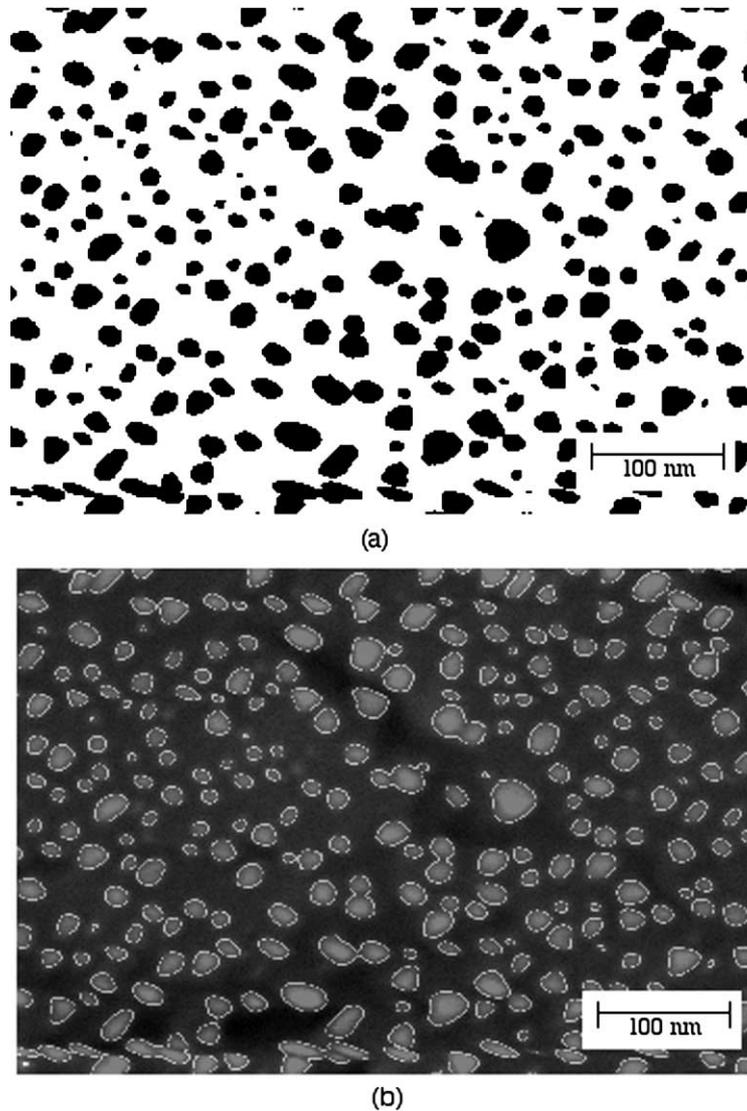


Fig. 2. Processed SEM image (a) converted black and white image; (b) particle outline overlaid on unprocessed image.

compared to the volume measured by the QCM during deposition.

For samples A–D, the results of these calculations, obtained from images of sufficient quality to perform the analysis, are also shown in Table 2. The volume fraction is

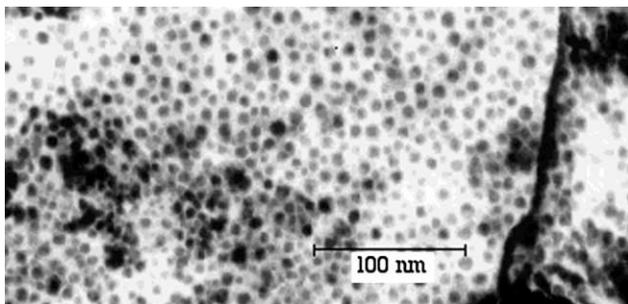


Fig. 3. TEM image of 1.5 nm of surface gold after 1 h at 400°C.

defined as the calculated volume divided by the nominal volume as estimated by the QCM. The annealing process is shown to decrease the number of particles per unit area and increase their size. The total volume of gold tends to remain constant but at about 50% of the volume as estimated by the QCM. An exception to this was evident for sample A. The images of this sample had poor contrast, due to the small amount of gold, which produced a large error in the measurement.

The discrepancy in gold volume could be accounted for by incorrect assumptions in the QCM measurement as discussed above. This measurement assumes the sticking coefficient of gold is the same for the QCM and the  $\text{WO}_3$  film. This may not be true, not only because of the difference in composition of the surfaces, but also because the surfaces are at different temperatures. At coverages this low, it is not possible to check the QCM calibration by profilometry. A QCM calibration by profilometry on a

Table 2  
Gold particle size analysis

Sample	Thermal history	Number density (no./ $\mu\text{m}^2$ )	Average particle area ( $\text{nm}^2$ )	Gold thickness by QCM ( $\text{nm}^2$ )	Volume fraction
A	3 h 400°C	–	–	0.8	–
	16 h 400°C	7800	40		1.2
	16 h 400°C, 7 h 600°C	640	180		0.83
B	3 h 400°C	–	–	1.6	–
	16 h 400°C	–	–		–
	16 h 400°C, 7 h 600°C	1000	150		0.51
C	3 h 400°C	5800	70	3.2	0.44
	16 h 400°C	3700	90		0.44
	16 h 400°C, 7 h 600°C	1400	190		0.47
D	1 h 400°C	10000	38	1.5	0.55

thicker gold layer would be based on the sticking coefficient of gold on gold.

The assumption of hemispherical shape for the gold particles may be inaccurate. If the particles are assumed to be closer to spherical in shape or prismatic, then the volume of gold calculated from the SEM images could be closer to the QCM value. However, from surface energy considerations, this is not likely [34].

The XPS data from sample E was used as another method to determine the volume of gold deposited on the  $\text{WO}_3$  surface. The as-deposited sample was assumed to have a

uniform coverage of gold as shown in Fig. 5. This assumption is based on the inability to observe gold particles on samples A, B, and C by SEM, prior to annealing.

The gold thickness was calculated from the Au 4f and W 4f peak area ratios using the following equation appropriate to a uniform overlayer (Fig. 5) where  $K$  is given by  $K = T\sigma\beta N$ .

$$\frac{I_{\text{Au}}}{I_{\text{W}}} = \frac{K_{\text{Au}} \int_0^d \exp(-z/\lambda_{\text{AuAu}}) dz}{K_{\text{W}} \exp(-d/\lambda_{\text{W Au}}) \int_0^\infty \exp(-z/\lambda_{\text{W WO}_3}) dz} \quad (1)$$

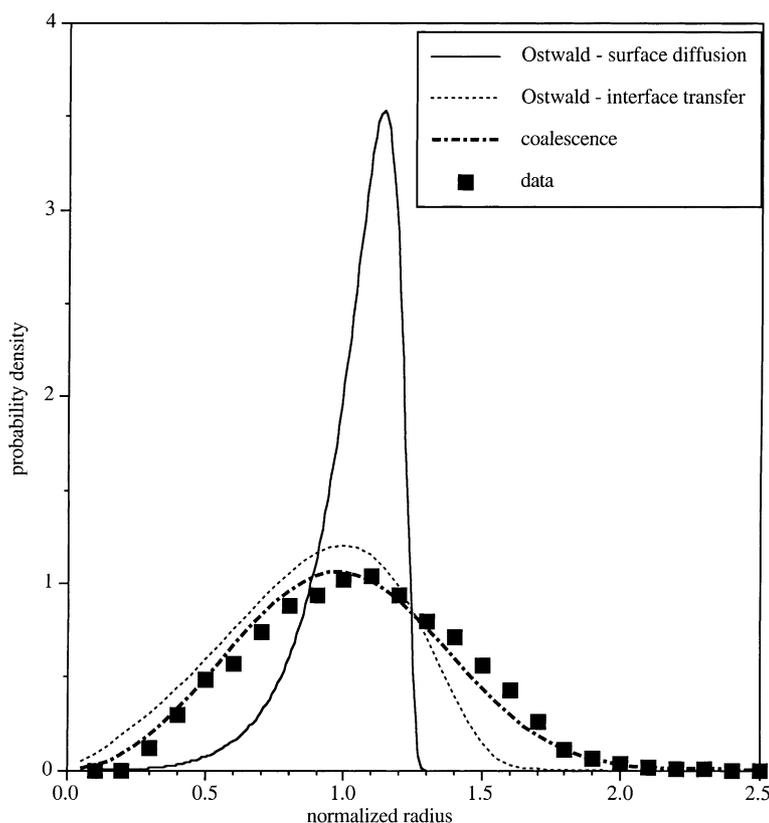


Fig. 4. Particle size distribution from the mean of 10 measurements on five samples compared to three model distributions.

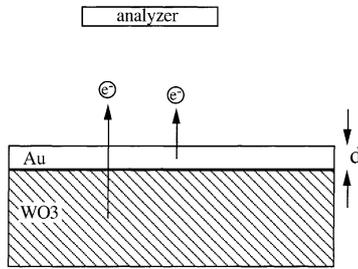


Fig. 5. XPS model for as-deposited gold (uniform coverage). The paths for photoelectrons emitted from Au and W are shown.

Literature values were used for the atom density,  $N$ , the angular asymmetry,  $\beta$  [35], and the photoionization cross-section,  $\sigma$  [36]. Either the inelastic mean free path (IMFP) [37] or the attenuation length (AL) [38] could be used in the calculations for the length scale,  $l$ . However, no value was available for the AL for  $\text{WO}_3$ , so only the inelastic mean free path was used. The length scale of the Au 4f photoelectrons in gold is designated as  $\lambda_{\text{AuAu}}$ , W 4f in  $\text{WO}_3$  as  $\lambda_{\text{W}\text{WO}_3}$ , and W 4f in gold as  $\lambda_{\text{W}\text{Au}}$ . The analyzer transmission function,  $T$ , for the Au 4f and W 4f photoelectrons was not known but the ratio was assumed to be proportional to the square root of the kinetic energies [39]. The value of  $d$  in Eq. (1) was adjusted until the intensity ratio was equal to the experimentally determined value. The value obtained for  $d$  was 0.77 nm or approximately 50% of the thickness as determined by the QCM. This agrees well with the volume fractions in Table 2 obtained by SEM analysis. We interpret this to be the initial sticking coefficient for gold on  $\text{WO}_3$  for the given deposition conditions as it falls within the range obtained for other metal/substrate systems [27,28].

The total annealing procedure for sample E was similar to that of samples A, B, and C. The peak area data taken after this procedure was analyzed as above but with the assumption that gold had formed hemispheres of equal radius,  $R$ , on the surface as shown in Fig. 6. The gold volume, as determined from  $d$  above and an assumed fractional coverage,  $\theta$  (i.e. the fraction of the  $\text{WO}_3$  surface covered by gold islands) fix the radius,  $R$ , and the number density,  $n$ , using the hemispherical assumption.

$$R = \frac{3d}{2\theta}, \quad n = \frac{\theta}{\pi} \left( \frac{2\theta}{3d} \right)^2 \quad (2)$$

$$\frac{I_{\text{Au}}}{I_{\text{W}}} = \frac{nK_{\text{Au}} \int_0^R 2\pi r \int_0^{\sqrt{R^2-r^2}} \exp(-z/\lambda_{\text{AuAu}}) dz dr}{K_{\text{W}} \lambda_{\text{W}\text{WO}_3} \left[ (1-\theta) + n \int_0^R 2\pi r \exp(-(\sqrt{R^2-r^2}/\lambda_{\text{W}\text{Au}})) dr \right]} \quad (3)$$

In this case,  $\theta$  was adjusted until the intensity ratio was equal to the experimentally determined value. The values of  $\theta$ ,  $d$ ,  $n$ , and the average particle area,  $A$ , are compared to the values obtained for sample B by SEM in Table 3. The thermal treatment of samples B and E was similar but not identical. While the total volume of gold is similar for both

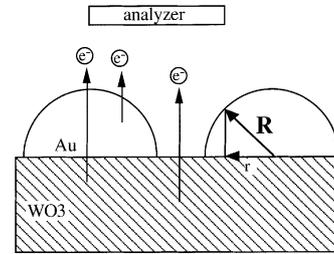


Fig. 6. XPS model after annealing. The paths for photoelectrons emitted from Au and W are shown.

Table 3  
Comparison of SEM and XPS results

	Sample B (SEM)	Sample E (XPS)
$q$	0.15	0.31
$d$ (nm)	0.82	0.77
$n$ (no./ $\mu\text{m}^2$ )	1000	7100
$A$ ( $\text{nm}^2$ )	150	44

the SEM and XPS methods, XPS tends to yield larger values for  $q$  and  $n$ , and smaller values for  $A$ .

#### 4. Conclusions

Both SEM and TEM images showed that for a gold coverage of less than several nanometers on polycrystalline  $\text{WO}_3$  films, aggregation into large particles occurs at temperatures above 400°C. The particles increase in size and the number density decreases over time. In order to accelerate aging, the annealing temperature used in these experiments was higher than the operating temperature often used in gas sensing applications. Nevertheless, the data show significant changes in the size and number density of surface gold particles in a short period of time compared to the many months that a sensing film may operate at elevated temperatures. Particle size distributions indicate that the growth mechanism is coalescence due to island mobility rather than Ostwald ripening.

Both SEM and XPS analysis indicate that the amount of gold deposited on the surface is approximately 50% of the value as determined by the QCM during deposition. This

difference is believed to be due to a low initial sticking probability of gold on the  $\text{WO}_3$  surface during deposition. At low coverages, it is not possible to check the QCM calibration by profilometry. The methods used in this paper may prove to be useful for the measurement of the actual amounts of metals deposited at low coverages. Surface analysis

methods such as demonstrated here may be necessary to understand and thus control the role of particle size in sensor response.

### Acknowledgements

Research at the Oak Ridge National Laboratory SHaRE User Facility was sponsored by the Division of Materials Sciences and Engineering, US Department of Energy, under contract DE-AC05-00OR22725 with UT-Battelle, LLC, and through the SHaRE Program under contract DE-AC05-76OR00033 with Oak Ridge Associated Universities. Portions of this work were supported by the Naval Surface Warfare Center, Dahlgren Division Grant No. 0178-99-1-9002.

### References

- [1] S.R. Morrison, Semiconductor gas sensors, *Sens. Actuators* 2 (1982) 329–341.
- [2] G. Hoogers, R. Huck, D. Kohl, G. Heiland, The uptake of oxygen by noble metal clusters on gas sensors, *Sens. Actuators B* 9 (1992) 123–125.
- [3] B. Frühberger, M. Grunze, D.J. Dwyer, Surface chemistry of H<sub>2</sub>S-sensitive tungsten oxide films, *Sens. Actuators B* 31 (1996) 167–174.
- [4] B. Frühberger, Interface chemistry of gold doped tungsten trioxide films in the reaction with hydrogen sulfide, Ph.D. Dissertation, Heidelberg, 1994.
- [5] B. Frühberger, M. Grunze, D.J. Dwyer, The formation and stability of sulfhydryl groups on the Au(1 1 0) surface, *J. Phys. Chem.* 98 (1994) 609–616.
- [6] J.F. Vetelino, R.K. Lade, R.S. Falconer, H<sub>2</sub>S surface acoustic wave sensor, *IEEE Trans. UFFC* 34 (1987) 156.
- [7] C.T. Campbell, Ultrathin metal films and particles on oxide surfaces: structural, electronic and chemisorptive properties, *Surf. Sci. Rep.* 27 (1997) 1–111.
- [8] G.C. Bond, The origins of particle size effects in heterogeneous catalysis, *Surf. Sci.* 156 (1985) 966–981.
- [9] M. Valden, X. Lai, D.W. Goodman, Onset of catalytic activity of gold clusters on titania with the appearance of non-metallic properties, *Science* 281 (1998) 1647–1650.
- [10] S.R. Morrison, Selectivity in semiconductor gas sensors, *Sens. Actuators* 12 (1987) 425–440.
- [11] S. Semancik, T.B. Fryberger, Model studies of SnO<sub>2</sub>-based gas sensors: vacancy defects and Pd additive effects, *Sens. Actuators B* 1 (1990) 97–102.
- [12] D.S. Sholl, R.T. Skodje, Late-stage coarsening of adlayers by dynamic cluster coalescence, *Physica A* 231 (1996) 631–647.
- [13] R.A. Dixon, R.G. Egdell, A study of the growth and mobility of Pd nanoclusters on WO<sub>3</sub>(0 0 1) by scanning tunneling microscopy, *Surf. Sci.* 452 (2000) 207–219.
- [14] J.R. Levine, J.B. Cohen, Y.W. Chung, Thin film island growth kinetics: a grazing incidence small angle X-ray scattering study of gold on glass, *Surf. Sci.* 248 (1991) 215–224.
- [15] L. Zhang, R. Persuad, T.E. Madey, Ultrathin metal films on a metal oxide surface: growth of Au on TiO<sub>2</sub>(1 1 0), *Phys. Rev. B* 56 (1997) 10549–10557.
- [16] W.B. Phillips, E.A. Desloge, J.G. Skofronick, A mechanism to account for observed morphological changes in discontinuous gold films following deposition, *J. Appl. Phys.* 39 (1968) 3210–3218.
- [17] J.G. Skofronick, W.B. Phillips, Morphological changes in discontinuous gold films following deposition, *J. Appl. Phys.* 38 (1967) 4791–4796.
- [18] M. Zinke-Allmang, L.C. Feldman, S. Nakahara, Role of Ostwald ripening in islanding processes, *Appl. Phys. Lett.* 51 (1987) 975–977.
- [19] M. Zinke-Allmang, L.C. Feldman, S. Nakahara, B.A. Davidson, Growth mechanism and clustering phenomena: the Ge-on-Si system, *Phys. Rev. B* 39 (1989) 7848–7851.
- [20] D.J. Semin, A. Lo, S.E. Roark, R.T. Skodje, K.L. Rowlen, Time-dependent morphology changes in thin silver films on mica: a scaling analysis of atomic force microscopy results, *J. Chem. Phys.* 105 (1996) 5542–5551.
- [21] K. Kinoshita, Mobility of small clusters on the substrate surface, *Thin Solid Films* 85 (1981) 223–238.
- [22] M.A. Listvan, Direct observations of small gold clusters and in situ cluster growth by STEM, *J. Mol. Catal.* 20 (1983) 265–278.
- [23] J.J. Metóis, K. Heinemann, H. Poppa, In situ investigation of the mobility of small gold clusters on cleaved MgO surfaces, *Appl. Phys. Lett.* 29 (1976) 134–136.
- [24] S. Nicoletti, L. Dori, G.C. Cardinali, A. Parisini, Gas sensors for air quality monitoring: realization and characterization of undoped and noble metal-doped SnO<sub>2</sub> thin sensing films deposited by the pulsed laser ablation, *Sens. Actuators* 60 (1999) 90–96.
- [25] S.C. Parker, A.W. Grant, V.A. Bondzie, C.T. Campbell, Island growth kinetics during the vapor deposition of gold onto TiO<sub>2</sub>(1 1 0), *Surf. Sci.* 441 (1999) 10–20.
- [26] J. Yoshihara, S.C. Parker, C.T. Campbell, Island growth kinetics during vapor deposition of Cu onto the Zn-terminated ZnO(0 0 1) surface, *Surf. Sci.* 439 (1999) 153–162.
- [27] X. Xu, D.W. Goodman, Metal deposition onto oxides: an unusual low sticking probability for copper on SiO<sub>2</sub>, *Appl. Phys. Lett.* 61 (1992) 1799–1801.
- [28] J.B. Zhou, H.C. Lu, T. Gustafsson, E. Garfunkel, Anomalously weak adsorption of Cu on SiO<sub>2</sub> and MgO surfaces, *Surf. Sci.* 293 (1993) L887–L892.
- [29] L.J. LeGore, R.J. Lad, J.F. Vetelino, B.G. Frederick, E.A. Kenik, in preparation.
- [30] S. Santucci, L. Lozzi, M. Passacantando, S.D. Nardo, A.R. Phani, C. Cantalini, M. Pelino, Study of the surface morphology and gas sensing properties of WO<sub>3</sub> thin films deposited by vacuum thermal evaporation, *J. Vac. Sci. Technol. A* 17 (1999) 644–649.
- [31] S. Barrett, *Image SXM*, Vol. 61, University of Liverpool, Liverpool, UK, 1997.
- [32] M. Vivino, National Institutes of Health.
- [33] B.K. Chakraverty, Grain size distribution in thin films. I. Conservative systems, *J. Phys. Chem. Solids* 28 (1967) 2401–2412.
- [34] M. Ohring, *The Materials Science of Thin Films*, Academic Press, San Diego, 1992.
- [35] R.F. Reilman, A. Msezane, S.T. Manson, Relative intensities in photoelectron spectroscopy of atoms and molecules, *J. Electron Spectrosc. Related Phenom.* 8 (1976) 389–394.
- [36] J.H. Scofield, Hartree–Slater subshell photoionization cross-sections at 1254 and 1487 eV, *J. Electron Spectrosc. Related Phenom.* 8 (1976) 129–137.
- [37] M.P. Seah, W.A. Dench, Quantitative electron spectroscopy of surfaces: a standard data base for electron inelastic mean free paths in solids, *Surf. Interface Anal.* 1 (1979) 2–11.
- [38] P.J. Cumpson, M.P. Seah, Elastic scattering corrections in AES and XPS. II. Estimating attenuation lengths and conditions required for their valid use in overlayer/substrate experiments, *Surf. Interface Anal.* 25 (1997) 430–446.
- [39] M.P. Seah, XPS reference procedure for the accurate intensity calibration of electron spectrometers: results of a BCR intercomparison co-sponsored by the VAMAS SCA TWA, *Surf. Interface Anal.* 20 (1993) 243–266.